



Sun, R., Carreira, S. C., Chen, Y., Xiang, C., Xu, L., Zhang, B., ... Rossiter, J. (2019). Stretchable Piezoelectric Sensing Systems for Self-Powered and Wireless Health Monitoring. *Advanced Materials Technologies*, 4(5), [1900100]. <https://doi.org/10.1002/admt.201900100>

Publisher's PDF, also known as Version of record

License (if available):
CC BY

Link to published version (if available):
[10.1002/admt.201900100](https://doi.org/10.1002/admt.201900100)

[Link to publication record in Explore Bristol Research](#)
PDF-document

This is the final published version of the article (version of record). It first appeared online via Wiley at <https://doi.org/10.1002/admt.201900100> . Please refer to any applicable terms of use of the publisher.

University of Bristol - Explore Bristol Research

General rights

This document is made available in accordance with publisher policies. Please cite only the published version using the reference above. Full terms of use are available:
<http://www.bristol.ac.uk/pure/about/ebr-terms>

Stretchable Piezoelectric Sensing Systems for Self-Powered and Wireless Health Monitoring

Rujie Sun, Sara Correia Carreira, Yan Chen, Chaoqun Xiang, Lulu Xu, Bing Zhang, Mudan Chen, Ian Farrow, Fabrizio Scarpa,* and Jonathan Rossiter*

Continuous monitoring of human physiological signals is critical to managing personal healthcare by early detection of health disorders. Wearable and implantable devices are attracting growing attention as they show great potential for real-time recording of physiological conditions and body motions. Conventional piezoelectric sensors have the advantage of potentially being self-powered, but have limitations due to their intrinsic lack of stretchability. Herein, a kirigami approach to realize a novel stretchable strain sensor is introduced through a network of cut patterns in a piezoelectric thin film, exploiting the anisotropic and local bending that the patterns induce. The resulting pattern simultaneously enhances the electrical performance of the film and its stretchability while retaining the mechanical integrity of the underlying materials. The power output is enhanced from the mechanoelectric piezoelectric sensing effect by introducing an intersegment, through-plane, electrode pattern. By additionally integrating wireless electronics, this sensing network could work in an entirely battery-free mode. The kirigami stretchable piezoelectric sensor is demonstrated in cardiac monitoring and wearable body tracking applications. The integrated soft, stretchable, and biocompatible sensor demonstrates excellent *in vitro* and *ex vivo* performances and provides insights for the potential use in myriad biomedical and wearable health monitoring applications.

device.^[1] Most tissues in the human body possess soft, curvilinear, and dynamic-deforming properties, while conventional sensors are generally based on rigid and stiff electronics that are mechanically incompatible with biological systems. To offer reliable and precise information of health, flexible and stretchable electronics that could conformably and compliantly interact at the surfaces of human skin and internal organs have received growing attention in recent years.^[2] There are generally two conceptually different strategies to achieve stretchability:^[3] on the one hand, recent advances in material synthesis provides a promising option to develop intrinsically stretchable materials, such as metal/ionic liquids,^[4] semiconductor/elastomer hybrid networks,^[5] and conductor/elastomer hybrid networks.^[6] Alternatively, in order to maintain the high electrical performance of conventional rigid materials, geometric designs are employed, such as mesh networks,^[7] wavy/buckled shapes,^[8] and segmented island-bridge layouts with serpentine^[9] or fractal^[10]


1. Introduction

Wearable electronics are attracting increasing attention as recent developments in materials, mechanics, and manufacturing techniques create new opportunities for the integration of high-quality electronic systems into a single miniaturized

interconnects. However, high cost and complexity of the fabrication process limit use and the required interconnect patterns would also occupy spaces, thus reducing the area density of active component. In recent years kirigami, the Japanese art of paper cutting has inspired materials scientists and mechanical designers to enhance the stretchability

R. Sun, Dr. B. Zhang, M. Chen, Dr. I. Farrow, Prof. F. Scarpa
Bristol Composites Institute (ACCIS)
University of Bristol
Bristol BS8 1TR, UK
E-mail: F.Scarpa@bristol.ac.uk

Dr. S. C. Carreira
School of Cellular and Molecular Medicine
University of Bristol
Bristol BS8 1TD, UK

 The ORCID identification number(s) for the author(s) of this article can be found under <https://doi.org/10.1002/admt.201900100>.

© 2019 The Authors. Published by WILEY-VCH Verlag GmbH & Co. KGaA, Weinheim. This is an open access article under the terms of the Creative Commons Attribution License, which permits use, distribution and reproduction in any medium, provided the original work is properly cited.

The copyright line of this paper was changed on 6 March 2019 after initial publication.

DOI: 10.1002/admt.201900100

Y. Chen
State Key Laboratory of Mechanics and Control of Mechanical Structures
Nanjing University of Aeronautics and Astronautics
Nanjing 210016, China

Dr. C. Xiang, Prof. J. Rossiter
Bristol Robotics Laboratory
University of Bristol
Bristol BS16 1QY, UK
E-mail: Jonathan.Rossiter@bristol.ac.uk

L. Xu
School of Materials
University of Manchester
Oxford Road, Manchester M13 9PL, UK

Prof. J. Rossiter
Department of Engineering Mathematics
University of Bristol
Bristol BS8 1UB, UK

in materials substrates. By exploiting kirigami topologies, a nonstretchable flat sheet can be transformed into an ultras-tretchable and conformable structure, while retaining its functional properties. The kirigami approach has been applied across a broad range of length scales, spanning from DNA kirigami at nanoscale,^[11] to graphene^[12] and nanocomposites^[13] at microscale, and various functional materials at macroscale.^[14–18] Another advantage of kirigami is that it could transform a variety of advanced materials and planar systems, that were previously limited in application, into mechanically tunable 2D and 3D architectures with broad geometric diversity.^[19] Kirigami techniques have been applied in a broad range of areas, including integrated solar tracking,^[14] deployable reflectors,^[15] energy storage devices,^[16] mechanical actuators,^[17] sensors,^[20] triboelectric nanogenerators,^[21] and stretchable electronics, such as conductors,^[22] supercapacitors,^[23] transistors,^[12] and bioprobes,^[24] and the stretchability can reach as high as 400% without degradation of intrinsic properties.

Rapid developments in sensing systems and biointegrated electronics have imposed a challenge on power sources, which are mainly based on batteries. Recently, self-powered systems have attracted much attention, and dedicated efforts have been made to develop energy-harvesting systems to extract energy from the body, as discussed in recent review papers.^[25,26] Among these power sources, mechanical energy is regarded as a promising option to offer sufficient power for embedded electronics.^[26] Many studies have aimed to develop mechanically flexible and biocompatible sensing and energy harvesting systems based on two commonly used techniques: piezoelectricity^[27,28] and triboelectricity.^[29] Piezoelectric sensors, the focus of this paper, exploit the mechanical-to-electrical conversion of piezo materials where electrical charge is induced upon mechanical strain. Inorganic materials are brittle and rigid in their bulk state, thus not inherently suitable to biomedical applications. Recently, however, efforts have been devoted to developing thin piezoelectric films of these materials in order to realize the needed flexibility, which normally involves complicated micro fabrication techniques.^[27] Alternatively, organic piezoelectric materials, such as polyvinylidene fluoride (PVDF), are preferable due to their natural flexibility.^[28] However, current designs based on piezoelectric sensors still retain a critical lack of stretchability, impeding applications in areas where large strains occur. For example, the dynamic strain of human skin could reach more than 30%,^[30] and most biological tissues exhibit moduli of tens to hundreds of kilopascal,^[31] much lower than the modulus of piezoelectric materials.

Here, inspired by the kirigami concept, we report an integrated stretchable sensing system in conjunction with wireless electronics for continuous health monitoring. This device is composed of two subsystems, a kirigami-based stretchable and self-powered sensing component, and a wireless communication interface for data transmission. A linear kirigami cut pattern is adopted for its simple manufacturing process. This design delivers significantly improved mechanical and electrical performances. Simulation analysis validates the superior mechanical properties of kirigami structures without inducing significant constraints on the measured surface compared with traditional planar structures. To enhance the sensing and power output of kirigami-based piezoelectric systems, a novel

intersegment electrode pattern is adopted and evaluated by a comparative study. The devices can be mounted on different surfaces as either wearable or implantable systems without mechanical irritation. The effectiveness of this approach for implantable devices is demonstrated by measuring the surface strain of a deforming balloon and ex vivo pig heart, and as a wearable sensor by measuring knee flexion. To demonstrate the capability for wireless sensing, an integrated sensing system with near-field communication (NFC) and self-powered capabilities is designed. Experiments with balloons and pig hearts illustrate the sensor signals under multiple conditions are successfully collected and wirelessly transmitted to external devices for real-time monitoring. We demonstrate that this type of sensing system with outstanding mechanical and electrical performances has great potential in future implantable and wearable healthcare applications.

2. Results and Discussion

2.1. Features of Integrated Sensing Systems

The stretchable sensing system introduced here provides a self-powered strain monitoring system with wireless communications for both implantable devices and wearable electronics. The key features of this system include its noninvasive conformity to various types of curved surfaces through a creative kirigami patterning and corresponding electrode interconnection design, and an interface based on NFC technology^[32] to wirelessly transmit strain information to external devices. **Figure 1a** gives the schematics of the kirigami sensing system for application in wireless cardiac monitoring. The device is composed of two subsystems: i) a stretchable piezoelectric film as the active sensing component to conform to the subject surface for strain measurements, and ii) a flexible and millimeter-scale wireless interface for NFC communications.

The whole wireless sensing system has a size of 28 mm × 60 mm, and can be easily mounted on various surfaces, and at many points on the human body (Figure 1b,c). As seen in the balloon demonstration (Figure 1b), this sensing system is compatible with curved and soft balloon surfaces without inducing extra constraints on the balloon deformations due to its high stretchability. The working principle is based on kirigami induced buckling. The structure stretches as the distance between two bonding areas increases, inducing the out-of-plane buckling of each strip. The induced bending of the piezoelectric films generates electrical power in d_{31} mode due to the piezoelectric effect. A stable wireless communication is created between the platform and a smartphone with NFC functionality even during the large dynamic deformations of the balloon. This platform is also demonstrated as a wearable device mounted on the human knees (Figure 1c), recording the daily activities and exercise. The kirigami induced 3D buckling could also be exploited to improve textile breathability, allowing heat and moisture vapor to be dissipated through the open structures. The developed sensor system delivers both a self-powered sensing function and wireless data transmit capability, two significant requirements for implantable electronics, e.g., for self-powered cardiac monitoring (Figure 1d).

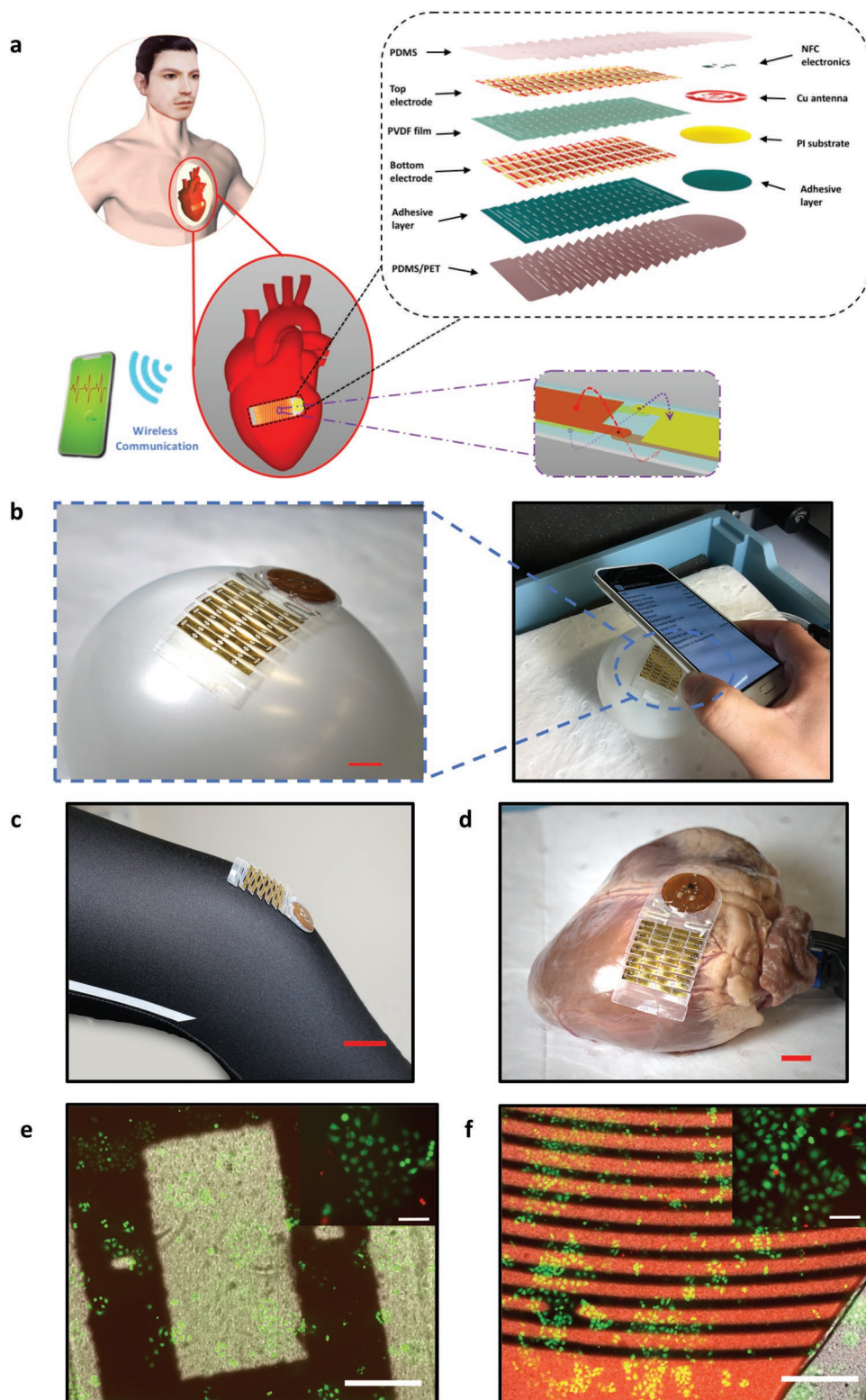


Figure 1. Schematic illustration, practical applications, and biocompatibility test of integrated self-powered sensing systems with wireless communication interface. a) Schematic illustration of the integrated device with multilayered structures between two subsystems: the stretchable sensor and wireless patch, and enlarged electrode patterns. b) Demonstration of the system on curved balloon surface with wireless communication capacity transmitting to external devices with NFC functionality, i.e., smartphone. Scale bar: 1 cm. c,d) Several potential application areas including skin (clothes) surface as wearable devices and tissue (pig heart) surface as implantable sensor. Scale bars 2 and 1 cm respectively. e,f) Biocompatibility tests. Live/dead staining of COS7 cells cultured on samples of the sensor (e) and communication part (f). Green fluorescence indicates live cells and red fluorescence shows dead cells. Insets show cells at a larger magnification. Scale bar of main images 0.5 mm, scale bar of insets 100 μm .

COS7 fibroblasts have been used as a generic cell model to investigate the biocompatibility of this sensing system. Here, COS7 cells have been cultured on samples of either the sensor or the communication part of the device and cell viability is measured after 24, 48, and 72 h of contact with the devices. COS7 cells have also been stained with calcein and ethidium homodimer III and imaged with a fluorescence microscope. Microscopy of the stained cell layers cultured on the sensor and communication devices for 48 h reveals that COS7 cells remain viable throughout the culture period (Figure 1e,f). This corroborates the results of the Alamar Blue assay and further confirms the biocompatibility of both device parts (Figure S1, Supporting Information).

2.2. Designs for Mechanical and Electrical Performances

A hyperelastic balloon, as a soft and stretchable surface demonstration, has been modeled using the finite element method (FEM) to explore the design of sensor structures. Two different patterns for sensors have been evaluated: one is a kirigami structure (Figure 2a), and the other is a commonly-used planar configuration (Figure 2b). The balloon is modeled using a neo-Hookean hyperelastic material using the commercial software Abaqus and the sensor structures are modeled as 2D shell elements. Nonlinear effects due to the larger deformation are considered during the analysis. These two sensor configurations have the same geometry in relaxed form, and both are bonded onto the balloon surface through tie constraints in the center of two opposite edges. The balloon has an initial 400 mL volume of water inside and is then inflated by an infusion process at a fixed filling speed to the final state with 450 mL water inside. In the final state, the kirigami structure has imposed less restrictions on the balloon inflation compared to the planar structure (Figure 2a,b). The maximum unwanted strain on the balloon surface with kirigami structure is 0.2, which is two times less than the 0.47 strain provided by the planar configuration. For a free balloon with no sensors, the average stress around the bonding area reaches 0.275 MPa. With the kirigami structure, the average stress is 0.328 MPa (an increase of 19.3%), while for the planar structure, the average stress is 0.822 MPa (a significantly larger increase of 198.8%) (Figure 2c). The free deformations are also compared under these three cases. The change of the arc distance between the two bonding areas is used to evaluate the deformation (Figure 2d). For the free balloon, the distance increases from 45.0 to 49.6 mm. The final distance with the kirigami structure is 49.0 mm, (a reduction of 13.0% compared to the free balloon). For the case of the planar structure, this change of distance is extremely small, from 45 to 45.04 mm (a reduction of 97%), meaning that the planar configuration severely restricts the deformation of the balloon. These comparative results demonstrate that a kirigami structure can efficiently mitigate the interfacial stress caused by the mismatch between rigid sensing electronics and soft biological surfaces.

Mechanical strength and electrical performance are generally two conflicting requirements in biointegrated electronics. Design optimization has also been performed on the electrode patterns of the piezoelectric sensors. 3D eight-node solid

element has been adopted for the sensor component, which consists in a two-layer structure: a 28 μm piezoelectric layer and a 75 μm plastic substrate. The electrode is not considered for the mechanical analysis. Three different configurations have been analyzed for comparison (Figure S2, Supporting Information): a kirigami structure with intersegment electrodes; another kirigami configuration with continuous electrodes; and a planar structure with continuous electrodes. The open-circuit voltages are calculated to evaluate the electrical performances with these three configurations (Figure 2e). The kirigami structure with continuous electrode structure shows the lowest voltage output, 0.19 V. This low performance is the result of charge cancellation in the kirigami-induced 3D buckling structures. The planar structure with continuous electrodes has a better electrical response, with an output voltage output of 1.26 V. The kirigami structure with intersegment electrodes, however, has a significantly increased open-circuit voltage (18.4 V). This remarkably large improvement in electrical performance is due to the reverse connections between adjacent segments, which serve to rectify and reinforce the charges between neighboring sensor segments with opposite bending direction (and hence opposite induced charge). When this type of intersegment electrodes is introduced the electrode areas would be slightly reduced due to the imperfections involved in the manufacturing process, thus inducing a small increase of the sensor impedance. Considering the electrode area effects, the charge outputs have been compared (Figure 2f), as calculated by

$$Q = \epsilon_r \times \epsilon_0 \times A \times V / t \quad (1)$$

where ϵ_0 is the air permittivity, $\epsilon_r = 12$ is the relative permittivity of piezoelectric film, t is the film thickness, V is the voltage output, and A is the electrode area. The electrode areas are 478.04, 835.18, and 933.5 mm^2 for the kirigami intersegment electrode, the kirigami continuous electrode, and the planar continuous electrode respectively. The charge output of the kirigami structure with intersegment electrodes is 3.33×10^{-8} C, which is 7.5 times larger than the value provided by the planar configuration with continuous electrodes (4.46×10^{-9} C), and 54 times larger than the one featured by the kirigami structure with the continuous electrodes (6.07×10^{-10} C).

2.3. Output Performances and Characterization

To evaluate the performance of the proposed sensing platform we have fabricated the stretchable sensor using the kirigami structural designs with the intersegment electrodes. The stretchability of this system is mainly attributed to the induced out-of-plane bending to accommodate the in-plane stretching (Figure 3a). The experimental results have also been replicated by FEM analysis. The electrical output has been analyzed before and after sensor encapsulation with polydimethylsiloxane (PDMS) (Figure 3b). Upon applying a sine-shape strain input at 1.5 Hz and 10% maximum strain amplitude, the open-circuit voltage (V_{oc}) and short-circuit current (I_{sc}) were 4.04 V and 6.16×10^{-8} A respectively before encapsulation, and

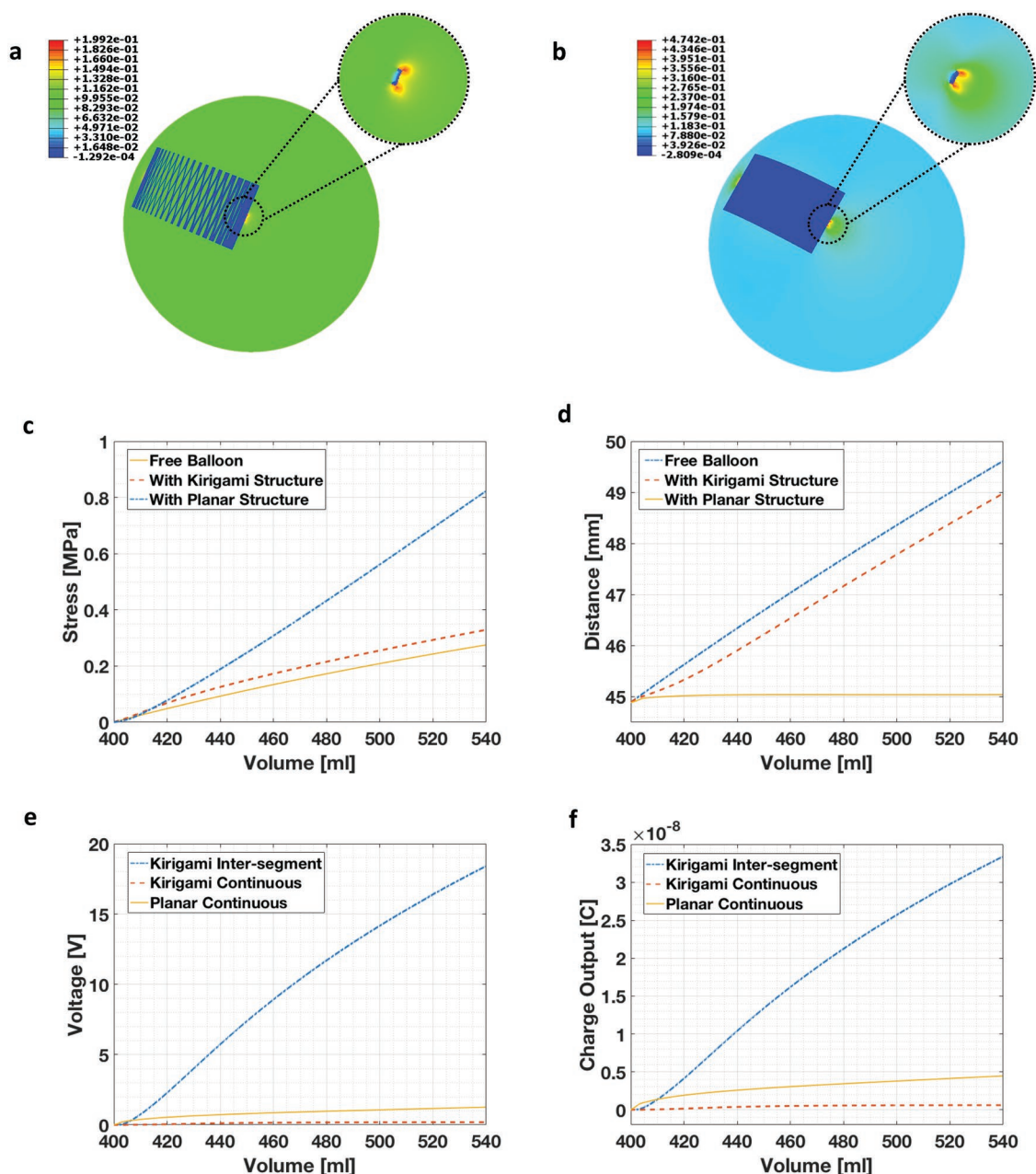


Figure 2. Mechanical and electrical optimization designs with simulation study. a,b) Two types of structures, kirigami and planar structures, on a curved balloon surface after its inflation showing strain distributions on the balloon surface around the bonding areas. c) A comparative study with the above two structural designs, and the average stress comparison around the bonding areas of the balloon during the inflation process in three cases: no sensing structure on balloon structure; Kirigami structure bonded to balloon surface; planar structure bonded to balloon surface. d) The distance change between two bonding areas during the balloon inflation process in the above three cases. e) Piezoelectric analysis of the electrode design for the sensing system in three designs: the kirigami structure with intersegment electrode pattern to reversely connect the adjacent segments to avoid charge cancellation; the kirigami structure with continuous electrode pattern; the planar structure with continuous electrode pattern. The voltage output during the balloon inflation process. f) The charge output considering the electrode areas in the above three cases in (e).

3.72 V and 5.70×10^{-8} A respectively after encapsulation. To evaluate the sensing performances in various conditions, the electrical outputs under a range of frequencies and strains were tested. Both V_{oc} and I_{sc} show a predominantly linear relationship within a frequency range of 0.5 to 3 Hz, and under strain amplitudes between 5% and 30% (Figure 3c and Figure S4, Supporting Information).

A cyclic tensile test has also been performed to validate the endurance of the sensing capabilities (Figure 3d). No notable change in voltage output is observed after 1500 cycles at 1.5 Hz, and the average output under three strain conditions, 10%, 15%, and 20% shows a linear relationship with the strain. The electrical performance of the piezoelectric sensor with the external resistors has also been investigated

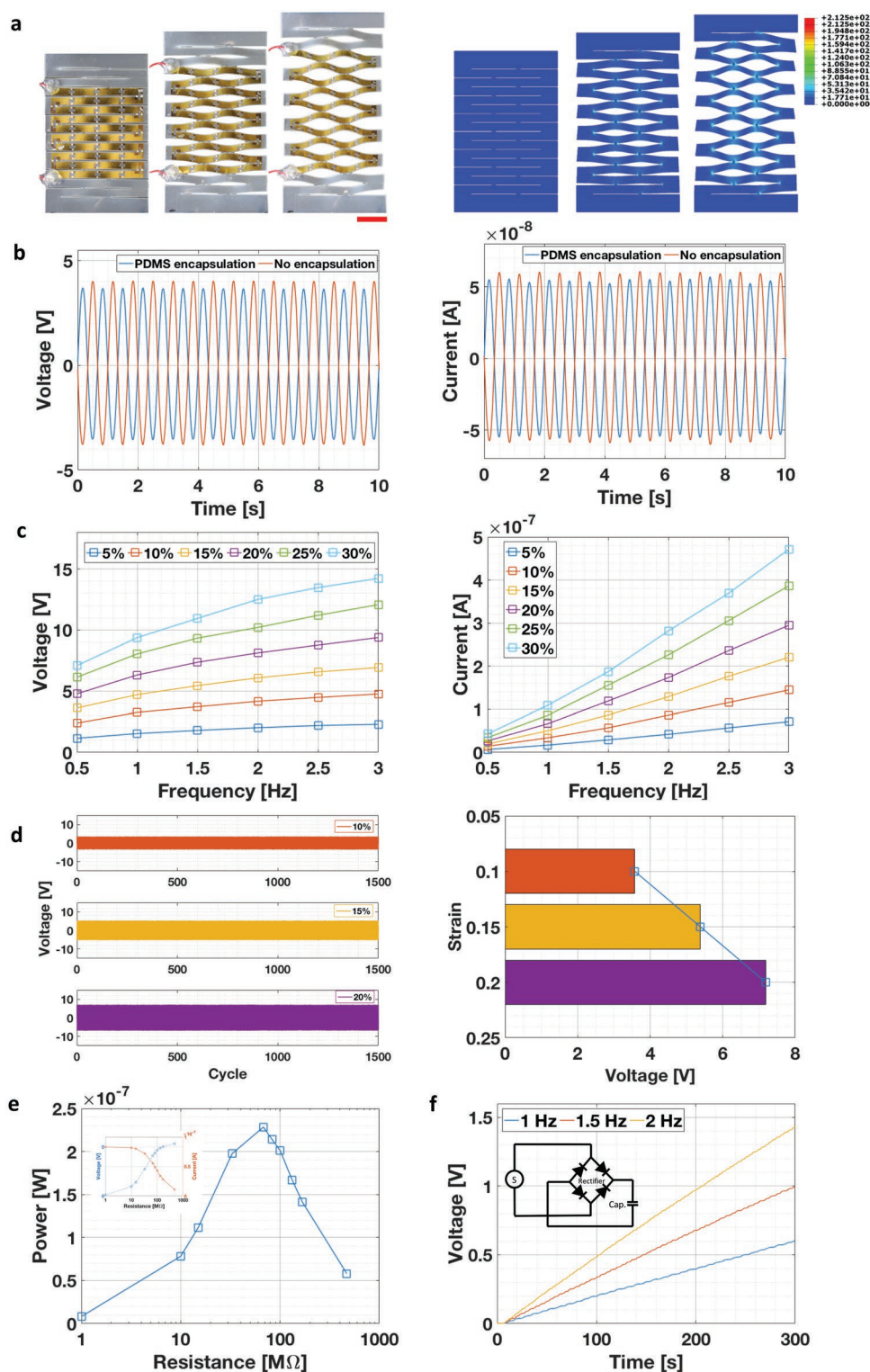


Figure 3. Electrical performance characterization of the sensing systems. a) (left) The different stages of the stretchable sensors under a tensile test. The strains are 0%, 15%, and 30% respectively. (right) The simulation results under the same three strains, and the stress distribution on the kirigami structure. Scale bar: 1 cm. b) The comparisons of the open-circuit voltage and short-circuit current versus time before and after PDMS encapsulation at 1.5 Hz and 10% strain. c) The open-circuit voltage and short-circuit current of the sensing system under a range of loading conditions, strain range from 5% to 30%, and frequency range from 0.5 to 3.0 Hz. d) A cycle test of the sensing system at 1.5 Hz and three strains: 10%, 15%, and 20%, and corresponding voltage amplitude comparison. e) The instantaneous power output calculated by the measured voltage and current from 1 to 470 $M\Omega$ at 1.5 Hz and 15% strain. The inset is the measured voltage and current output under different load resistances. f) The charging of a capacitor (10 μF) from the rectified voltage output of the sensor under 15% strain. The inset is the circuit diagram of the energy harvesting and storage system.

to assess the instantaneous power output at 1.5 Hz and 15% strain (Figure 3e). The load resistors range between 1 and 470 M Ω ; the voltage increases with the resistance and reaches 5.32 V when the resistance is 470 M Ω , which is close to its corresponding V_{oc} of 5.44 V. The current decreases as the resistance increases, with a value of 8.32×10^{-8} A at 1 M Ω that is also close to its corresponding I_{sc} of 8.66×10^{-8} A. The output power is calculated by multiplying the measured voltage and current, reaching a maximum of 228 nW under the load resistance of 68 M Ω . Energy harvesting performance is also an important characteristic for self-powered sensors, and the collected energy could also be used as a supplementary power source for other implantable devices such as pacemakers. A 10 μ F capacitor has been used to store the harvested energy from the mechanical deformation (Figure 3f). A silicon bridge rectifier is used to convert the piezoelectric AC output to DC signals before charging the capacitor, and three different frequencies (1, 1.5, and 2 Hz) at 15% strain amplitude have been applied to investigate the charge performance. The sensor could charge the capacitor to 1 V within 200 s at a frequency of 2 Hz. These results indicate that the featured sensing system is a promising stretchable self-powered sensor for implantable electronics applications.

2.4. Sensing Capability Assessment in Multiple Conditions

To further validate the functionality of the device, a series of tests, including *in vitro*, *ex vivo*, and *on body*, have been performed. Two types of fluid, air and water, have been infused into a balloon to inflate it through a controllable setup (Figure 4ai,ii). In the air-driven platform, a pressure gauge is used to record the pressure change inside the balloon, and the sensor outputs varying with the pressure change are subsequently analyzed. The kirigami sensor conforms to the balloon surface well while still maintaining its free deformations (Figure 4bi,ii). Two types of control signals (sine and heartbeat-like shapes) have been applied to the syringe movements to evaluate the sensing performance with balloon deformations under various conditions. For the case of sine wave inflation, with increasing frequency and pressure (4.0 to 5.7 kPa and 0.5 to 1.5 Hz, respectively), the voltage outputs increase linearly (Figure 4c and Figure S8, Supporting Information). For the case of the heartbeat-like inflation, the detailed characteristics of balloon expansion and contraction are replicated in the voltage signals (Figure 4d). Linear relationships between the sensor output and frequency and pressure have been obtained (Figure S8, Supporting Information) in the range of frequencies 0.5 to 1.5 Hz and pressures 3.4 to 4.4 kPa. For water as the infusion material, a flowmeter is used to record the volume change of the balloon. The results illustrate that the sensor output changes with a linear relationship with the change of frequency and water volume (Figures S9 and S10, Supporting Information).

Ex vivo tests are also performed using the *in vitro* test set-up by substituting the balloon with a fresh pig heart to simulate the *in vivo* environment. One chamber of the heart is inflated by either water or air. The sensor shows a good conformability to the pig heart surface before and after deformation (Figure 4biii,iv). Two types of signals, pulse (Figure 4e) and

heartbeat-like (Figure 4f) shapes, have been applied to inflate the heart under a range of frequencies and pressures using air. For the heartbeat-like input, the characteristics of the heart deformations in diastole and systole are clearly embodied in the signal outputs. The average amplitude of the generated voltage also features a linear relationship with pressure and frequency for the pulse waveform (Figure S11, Supporting Information). A similar relationship between the voltage output and the infused water volume and applied frequency is observed for the water-driven case (Figure S12, Supporting Information).

In addition to reliable applications for implantable devices, this sensing system also shows great potential for wearable electronics to record daily activities. To monitor daily exercises, this sensor can be readily mounted on body joints where large deformation occurs, such as the knees (Figure 4bv,vi). Different types of exercises, including cycle, running, and climbing, have been performed to evaluate the sensing performance. For each type of motion, the device illustrates a clearly different voltage waveform, which provided a facile way to distinguish the motion type (Figure 4g). In addition, when the running speed increases gradually, the voltage amplitude shows a gradual increase (Figure 4h). Moreover, due to the open 3D buckling structure introduced by kirigami cutting, the design featured here is intrinsically breathable, and can therefore be incorporated into performance textiles where breathability is essential.

2.5. Assessment of Integrated Systems for Wireless Sensing Capacities

Considering implantable biomedical devices in real applications, wireless communication is an indispensable capability. NFC technology is therefore explored for integration with our kirigami sensor to collect the strain outputs and transmit the data to external devices. This provides a convenient way to monitor *in-body* and *on-body* conditions in real-time with portable devices, such as a smart phone with NFC functionality. A miniaturized wireless interface with the radius of ≈ 8 mm have been designed and fabricated (Figure 5a) to capture and transmit the analog voltage signal from the sensor, and an external NFC reader is used to acquire the data. For *in vitro* assessment, the previously described air-driven testing platform is used to demonstrate the wireless communication abilities. The sensor is directly connected to the wireless interface using two signal wires. Similar tests as above for balloon deformations under a series of frequencies and pressures have been performed to evaluate the performance of the integrated sensor-communication system. For a fixed balloon pressure, the signal output acquired from the NFC reader is stable, and its amplitude increases with an increase in frequency (Figure 5b). The results from the wireless NFC interface are then compared with those using wired connections to an oscilloscope, and the results from the two measuring methods are consistent with each other (Figure S16, Supporting Information). A heartbeat-like input has also been applied to simulate the real heart beating, and the results from the wireless interface illustrated its successful acquisition of the signal characteristics at a representative frequency of 1 Hz (Figure 5c). The trend of the voltage/pressure signals match the sensor signal obtained from the wired platform.

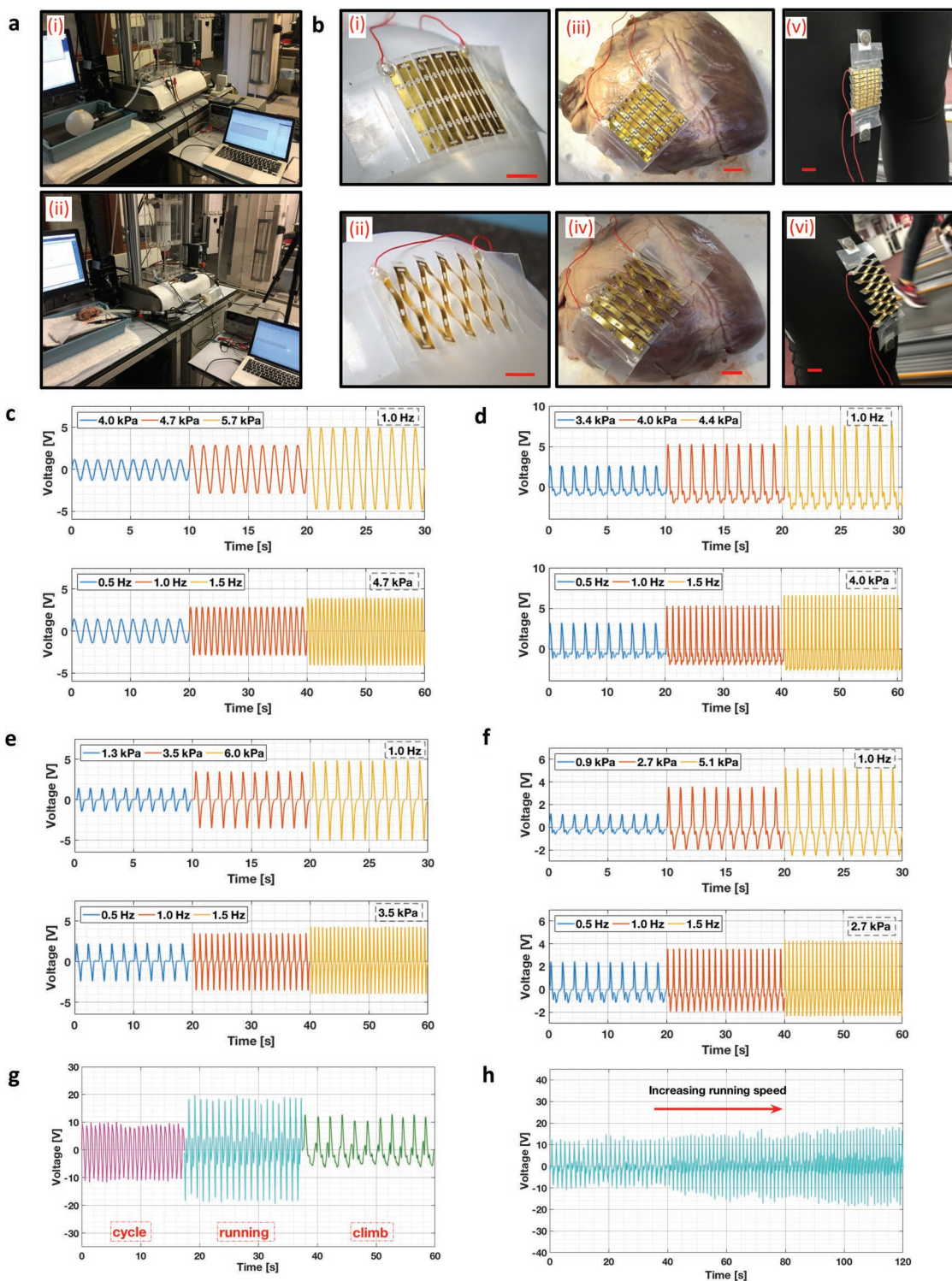


Figure 4. The application tests of the sensing system in multiple conditions. a) The setup for the in vitro and ex vivo test with air and water as the infusion medium respectively. b) The use of the stretchable sensor on a range of curved surfaces, including balloon, pig heart, and knee joint. The conditions of its initial and deformed states. Scale bar: 1 cm. c) The voltage output of the sensor bonded to the balloon under different frequencies and pressures for a sine-shape input on air-driven platform. d) The voltage output of the sensor on the balloon under different frequencies and pressures under a heartbeat-like input on air-driven platform. e, f). The voltage output of the sensor on the pig heart under different frequencies and pressures with pulse and heartbeat-like inputs on air-driven platform. g) The voltage output of the sensor mounting on the knee areas for three types of exercise: cycling, running, and climbing. h) The voltage output of the sensor when the running speed increases gradually.

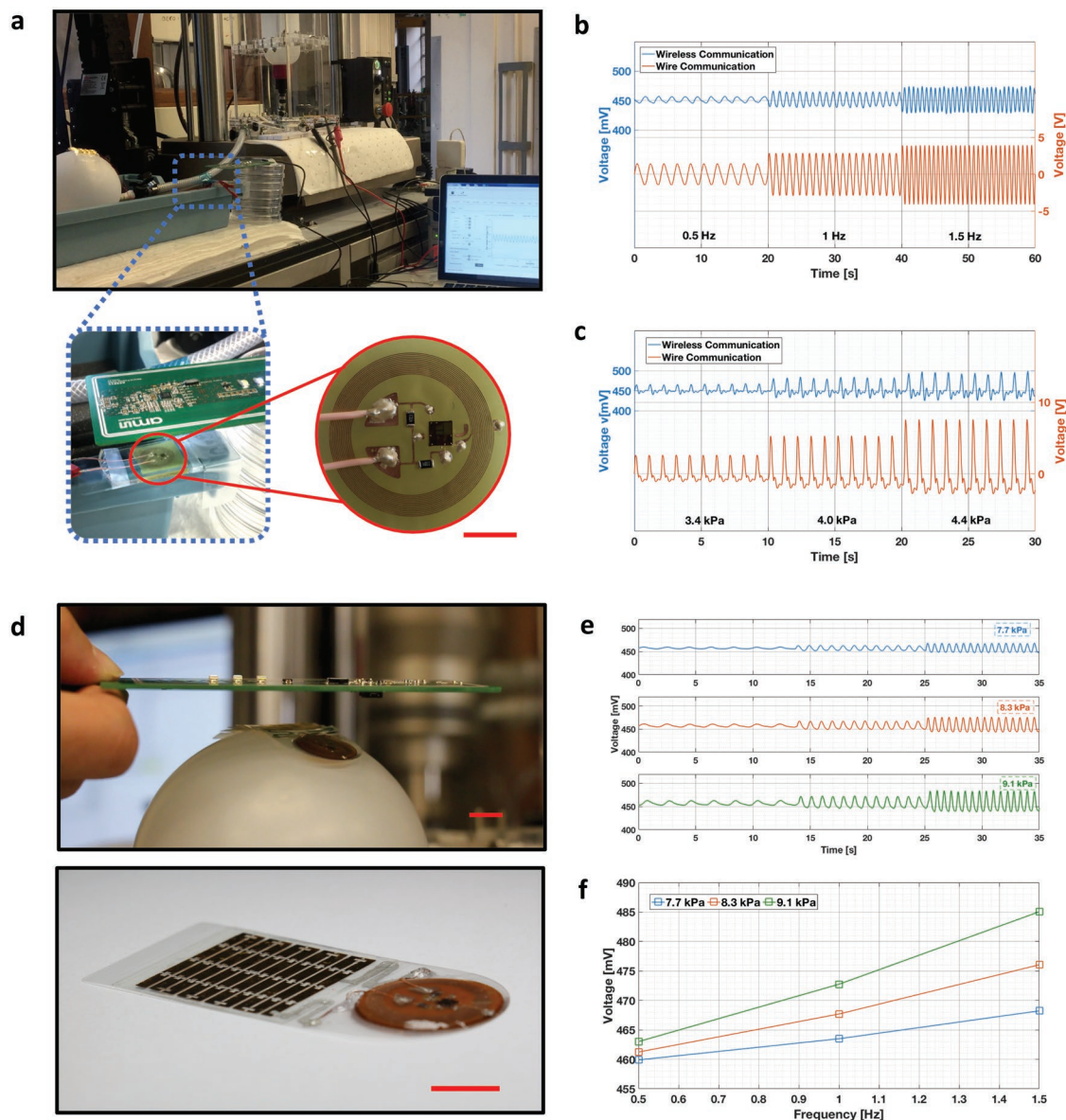


Figure 5. The wireless communication assessment of the integrated system. a) The setup for the comparison between wire and wireless results. Enlarged images show the wireless patch, and the communication between the wireless patch and external reader. Scale bar: 5 cm. b) The comparative results between the wire and wireless measurement methods with sine-wave input under 4.0 kPa and three frequencies: 0.5, 1.0, and 1.5 Hz on air-driven platform. c) The comparative results between the wire and wireless measurement methods with heartbeat-like input at 1 Hz and for three pressures. d) The fully integrated sensing and communication system, and its evaluation on the balloon surface. Scale bar: 2 and 1 cm. e, f) The wirelessly transmitted data from the integrated system under a series of conditions, including frequency and pressure changes, and the voltage amplitude comparison with the changing parameters.

Finally, we demonstrate the complete self-contained biosensor by integrating the kirigami sensor and NFC interface into a single module (Figure 5d). The sensor size is further optimized to match the dimension of the wireless component to achieve a miniaturized and flexible integrated sensing system. A series of tests has been performed to evaluate the operation of this integrated system at three frequencies and three pressures (Figure 5e). The acquired results validate the reliability of this integrated system and illustrate the near-linear relationship between the input (frequency and pressure) and output (voltage) (Figure 5f).

3. Conclusion

In conclusion, the flexible and stretchable integrated sensing system presented here represents a significant technology advance to achieve self-powered and wireless health monitoring. The structural flexibility allows this system to robustly conform to various curved surfaces, including the balloon, heart surface, and body joints. Compared to previously reported methods for stretchability, the kirigami technique provides a straightforward method to achieve compliance by a tailored cutting pattern, simplifying the microfabrication process. By

introducing a novel intersegment electrode design, this integrated sensing system shows advantages in both mechanical and electrical performances. Another attractive feature of the proposed system is the miniaturized wireless interface allowing the sensing data to be transmitted to an external device wirelessly, which is of vital importance to implantable devices. In addition to the systematic modeling of the devices, a range of practical assessments, including *in vitro*, *ex vivo*, and on body, have been performed. With the integration of the NFC functionality, the collected data are transmitted to external devices to achieve wireless and real-time health monitoring with no power needed for the sensor or the communication chip. These features contribute to the effectiveness of the developed wireless and self-powered sensing platform and differentiate it from other sensing systems. The developed device has the potential to significantly expand the wireless monitoring of vital signs and important biomechanical indicators of health.

4. Experimental Section

Materials and Methods and any associated references are presented in the Supporting Information.

Supporting Information

Supporting Information is available from the Wiley Online Library or from the author.

Acknowledgements

This work was supported by the Engineering and Physical Sciences Research Council through the EPSRC Centre for Doctoral Training in Advanced Composites for Innovation and Science (Grant No. EP/L016028/1). R.S. acknowledges the support from the China Scholarship Council. J.R. was supported by EPSRC Grant Nos. EP/M020460/1, EP/M026388/1, and EP/R02961X/1, and the Royal Academy of Engineering under the Chair in Emerging Technologies scheme. S.C.C. acknowledges the Wolfson Bioimaging Facility at the University of Bristol for access to fluorescence microscopy. Data are available at the University of Bristol data repository. <https://doi.org/10.5523/bris.360lx9c6dpohh2ncr64uuqmq9s>.

Conflict of Interest

The authors declare no conflict of interest.

Keywords

kirigami, metamaterials, near-field communication, piezoelectric sensors

Received: January 30, 2019

Published online:

[1] a) D.-H. Kim, N. Lu, R. Ma, Y.-S. Kim, R.-H. Kim, S. Wang, J. Wu, S. M. Won, H. Tao, A. Islam, K. J. Yu, T.-i. Kim, R. Chowdhury,

- M. Ying, L. Xu, M. Li, H.-J. Chung, H. Keum, M. McCormick, P. Liu, Y.-W. Zhang, F. G. Omenetto, Y. Huang, T. Coleman, J. A. Rogers, *Science* **2011**, 333, 838; b) W. Gao, S. Emaminejad, H. Y. Y. Nyein, S. Challa, K. Chen, A. Peck, H. M. Fahad, H. Ota, H. Shiraki, D. Kiriya, D.-H. Lien, G. A. Brooks, R. W. Davis, A. Javey, *Nature* **2016**, 529, 509; c) D. Son, J. Lee, S. Qiao, R. Ghaffari, J. Kim, J. E. Lee, C. Song, S. J. Kim, D. J. Lee, S. W. Jun, S. Yang, M. Park, J. Shin, K. Do, M. Lee, K. Kang, C. S. Hwang, N. Lu, T. Hyeon, D.-H. Kim, *Nat. Nanotechnol.* **2014**, 9, 397.
- [2] M. Kapnisi, C. Mansfield, C. Marijon, A. G. Guex, F. Perbellini, I. Bardi, E. J. Humphrey, J. L. Puetzer, D. Mawad, D. C. Koutsogeorgis, D. J. Stuckey, C. M. Terracciano, S. E. Harding, M. M. Stevens, *Adv. Funct. Mater.* **2018**, 28, 1800618.
- [3] J. A. Rogers, T. Someya, Y. Huang, *Science* **2010**, 327, 1603.
- [4] H. Ota, K. Chen, Y. Lin, D. Kiriya, H. Shiraki, Z. Yu, T.-J. Ha, A. Javey, *Nat. Commun.* **2014**, 5, 5032.
- [5] J. Xu, S. Wang, G.-J. N. Wang, C. Zhu, S. Luo, L. Jin, X. Gu, S. Chen, V. R. Feig, J. W. F. To, S. Rondeau-Gagné, J. Park, B. C. Schroeder, C. Lu, J. Y. Oh, Y. Wang, Y.-H. Kim, H. Yan, R. Sinclair, D. Zhou, G. Xue, B. Murmann, C. Linder, W. Cai, J. B. H. Tok, J. W. Chung, Z. Bao, *Science* **2017**, 355, 59.
- [6] D. J. Lipomi, M. Vosgueritchian, B. C. K. Tee, S. L. Hellstrom, J. A. Lee, C. H. Fox, Z. Bao, *Nat. Nanotechnol.* **2011**, 6, 788.
- [7] T. Someya, Y. Kato, T. Sekitani, S. Iba, Y. Noguchi, Y. Murase, H. Kawaguchi, T. Sakurai, *Proc. Natl. Acad. Sci. USA* **2005**, 102, 12321.
- [8] D.-Y. Khang, H. Jiang, Y. Huang, J. A. Rogers, *Science* **2006**, 311, 208.
- [9] a) D.-H. Kim, J. Song, W. M. Choi, H.-S. Kim, R.-H. Kim, Z. Liu, Y. Y. Huang, K.-C. Hwang, Y.-w. Zhang, J. A. Rogers, *Proc. Natl. Acad. Sci. USA* **2008**, 105, 18675; b) N. Lu, C. Lu, S. Yang, J. Rogers, *Adv. Funct. Mater.* **2012**, 22, 4044.
- [10] a) S. Xu, Y. Zhang, J. Cho, J. Lee, X. Huang, L. Jia, J. A. Fan, Y. Su, J. Su, H. Zhang, H. Cheng, B. Lu, C. Yu, C. Chuang, T.-i. Kim, T. Song, K. Shigeta, S. Kang, C. Dagdeviren, I. Petrov, P. V. Braun, Y. Huang, U. Paik, J. A. Rogers, *Nat. Commun.* **2013**, 4, 1543; b) J. A. Fan, W.-H. Yeo, Y. Su, Y. Hattori, W. Lee, S.-Y. Jung, Y. Zhang, Z. Liu, H. Cheng, L. Falgout, M. Bajema, T. Coleman, D. Gregoire, R. J. Larsen, Y. Huang, J. A. Rogers, *Nat. Commun.* **2014**, 5, 3266.
- [11] D. Han, S. Pal, Y. Liu, H. Yan, *Nat. Nanotechnol.* **2010**, 5, 712.
- [12] M. K. Bles, A. W. Barnard, P. A. Rose, S. P. Roberts, K. L. McGill, P. Y. Huang, A. R. Ruyack, J. W. Kevek, B. Kobrin, D. A. Muller, P. L. McEuen, *Nature* **2015**, 524, 204.
- [13] T. C. Shyu, P. F. Damasceno, P. M. Dodd, A. Lamoureux, L. Xu, M. Shlian, M. Shtein, S. C. Glotzer, N. A. Kotov, *Nat. Mater.* **2015**, 14, 785.
- [14] A. Lamoureux, K. Lee, M. Shlian, S. R. Forrest, M. Shtein, *Nat. Commun.* **2015**, 6, 8092.
- [15] a) W. Wang, C. Li, H. Rodrigue, F. P. Yuan, M. W. Han, M. Cho, S. H. Ahn, *Adv. Funct. Mater.* **2017**, 27, 1604214; b) Y. Tang, G. Lin, S. Yang, Y. K. Yi, R. D. Kamien, J. Yin, *Adv. Mater.* **2017**, 29, 1604262.
- [16] H. Guo, M. H. Yeh, Y. C. Lai, Y. Zi, C. Wu, Z. Wen, C. Hu, Z. L. Wang, *ACS Nano* **2016**, 10, 10580.
- [17] M. A. Dias, M. P. McCarron, D. Rayneau-Kirkhope, P. Z. Hanakata, D. K. Campbell, H. S. Park, D. P. Holmes, *Soft Matter* **2017**, 13, 9087.
- [18] X. Wang, X. Guo, J. Ye, N. Zheng, P. Kohli, D. Choi, Y. Zhang, Z. Xie, Q. Zhang, H. Luan, K. Nan, B. H. Kim, Y. Xu, X. Shan, W. Bai, R. Sun, Z. Wang, H. Jang, F. Zhang, Y. Ma, Z. Xu, X. Feng, T. Xie, Y. Huang, Y. Zhang, J. A. Rogers, *Adv. Mater.* **2018**, 0, 1805615.
- [19] a) Y. Zhang, Z. Yan, K. Nan, D. Xiao, Y. Liu, H. Luan, H. Fu, X. Wang, Q. Yang, J. Wang, W. Ren, H. Si, F. Liu, L. Yang, H. Li, J. Wang, X. Guo, H. Luo, L. Wang, Y. Huang, J. A. Rogers, *Proc. Natl. Acad. Sci. USA* **2015**, 112, 11757; b) R. M. Neville, F. Scarpa, A. Pirrera, *Sci. Rep.* **2016**, 6, 31067.

- [20] R. Sun, B. Zhang, L. Yang, W. Zhang, I. Farrow, F. Scarpa, J. Rossiter, *Appl. Phys. Lett.* **2018**, *112*, 251904.
- [21] C. Wu, X. Wang, L. Lin, H. Guo, Z. L. Wang, *ACS Nano* **2016**, *10*, 4652.
- [22] a) Z. Wang, L. Zhang, S. Duan, H. Jiang, J. Shen, C. Li, *J. Mater. Chem. C* **2017**, *5*, 8714; b) J. Lyu, M. D. Hammig, L. Liu, L. Xu, H. Chi, C. Uher, T. Li, N. A. Kotov, *Appl. Phys. Lett.* **2017**, *111*, 161901.
- [23] a) Z. Lv, Y. Luo, Y. Tang, J. Wei, Z. Zhu, X. Zhou, W. Li, Y. Zeng, W. Zhang, Y. Zhang, D. Qi, S. Pan, X. J. Loh, X. Chen, *Adv. Mater.* **2018**, *30*, 1704531; b) R. Xu, A. Zverev, A. Hung, C. Shen, L. Irie, G. Ding, M. Whitmeyer, L. Ren, B. Griffin, J. Melcher, L. Zheng, X. Zang, M. Sanghadasa, L. Lin, *Microsyst. Nanoeng.* **2018**, *4*, 36.
- [24] Y. Morikawa, S. Yamagiwa, H. Sawahata, R. Numano, K. Koida, M. Ishida, T. Kawano, *Adv. Healthcare Mater.* **2018**, *7*, 1701100.
- [25] a) A. Proto, M. Penhaker, S. Conforto, M. Schmid, *Trends Biotechnol.* **2017**, *35*, 610; b) C. Dagdeviren, Z. Li, Z. L. Wang, *Annu. Rev. Biomed. Eng.* **2017**, *19*, 85; c) M. A. Parvez Mahmud, N. Huda, S. H. Farjana, M. Asadnia, C. Lang, *Adv. Energy Mater.* **2018**, *8*, 1701210.
- [26] Q. Zheng, B. Shi, Z. Li, Z. L. Wang, *Adv. Sci.* **2017**, *4*, 1700029.
- [27] a) D. H. Kim, H. J. Shin, H. Lee, C. K. Jeong, H. Park, G.-T. Hwang, H.-Y. Lee, D. J. Joe, J. H. Han, S. H. Lee, J. Kim, B. Joung, K. J. Lee, *Adv. Funct. Mater.* **2017**, *27*, 1700341; b) C. Dagdeviren, B. D. Yang, Y. Su, P. L. Tran, P. Joe, E. Anderson, J. Xia, V. Doraiswamy, B. Dehdashti, X. Feng, B. Lu, R. Poston, Z. Khalpey, R. Ghaffari, Y. Huang, M. J. Slepian, J. A. Rogers, *Proc. Natl. Acad. Sci. USA* **2014**, *111*, 1927; c) C. Dagdeviren, F. Javid, P. Joe, T. von Erlach, T. Bense, Z. Wei, S. Saxton, C. Cleveland, L. Booth, S. McDonnell, J. Collins, A. Hayward, R. Langer, G. Traverso, *Nat. Biomed. Eng.* **2017**, *1*, 807.
- [28] a) H. Zhang, X.-S. Zhang, X. Cheng, Y. Liu, M. Han, X. Xue, S. Wang, F. Yang, A. S. Smitha, H. Zhang, Z. Xu, *Nano Energy* **2015**, *12*, 296; b) B. Xu, X. Lin, W. Li, Z. Wang, W. Zhang, P. Shi, *Adv. Funct. Mater.* **2017**, *27*, 1606169.
- [29] a) Q. Zheng, H. Zhang, B. Shi, X. Xue, Z. Liu, Y. Jin, Y. Ma, Y. Zou, X. Wang, Z. An, W. Tang, W. Zhang, F. Yang, Y. Liu, X. Lang, Z. Xu, Z. Li, Z. L. Wang, *ACS Nano* **2016**, *10*, 6510; b) Y. Ma, Q. Zheng, Y. Liu, B. Shi, X. Xue, W. Ji, Z. Liu, Y. Jin, Y. Zou, Z. An, W. Zhang, X. Wang, W. Jiang, Z. Xu, Z. L. Wang, Z. Li, H. Zhang, *Nano Lett.* **2016**, *16*, 6042; c) Q. Zheng, B. Shi, F. Fan, X. Wang, L. Yan, W. Yuan, S. Wang, H. Liu, Z. Li, Z. L. Wang, *Adv. Mater.* **2014**, *26*, 5851.
- [30] A. M. Wessendorf, D. J. Newman, *IEEE Trans. Biomed. Eng.* **2012**, *59*, 3432.
- [31] X. Yu, H. Wang, X. Ning, R. Sun, H. Albadawi, M. Salomao, A. C. Silva, Y. Yu, L. Tian, A. Koh, C. M. Lee, A. Chempakasseril, P. Tian, M. Pharr, J. Yuan, Y. Huang, R. Oklu, J. A. Rogers, *Nat. Biomed. Eng.* **2018**, *2*, 165.
- [32] a) A. Koh, D. Kang, Y. Xue, S. Lee, R. M. Pielak, J. Kim, T. Hwang, S. Min, A. Banks, P. Bastien, M. C. Manco, L. Wang, K. R. Ammann, K.-I. Jang, P. Won, S. Han, R. Ghaffari, U. Paik, M. J. Slepian, G. Balooch, Y. Huang, J. A. Rogers, *Sci. Transl. Med.* **2016**, *8*, 366ra165; b) J. Kim, G. A. Salvatore, H. Araki, A. M. Chiarelli, Z. Xie, A. Banks, X. Sheng, Y. Liu, J. W. Lee, K.-I. Jang, S. Y. Heo, K. Cho, H. Luo, B. Zimmerman, J. Kim, L. Yan, X. Feng, S. Xu, M. Fabiani, G. Gratton, Y. Huang, U. Paik, J. A. Rogers, *Sci. Adv.* **2016**, *2*, e1600418.